Polymer 50 (2009) 913–921

Contents lists available at ScienceDirect

Polymer

journal homepage: www.elsevier.com/locate/polymer

Poly(ethylene terephthalate) nanofibers prepared by CO_2 laser supersonic drawing

Akihiro Suzuki*, Ken Tanizawa

Interdisciplinary Graduate School of Medicine and Engineering, University of Yamanashi, Takeda-4, Kofu 400-8511, Japan

ARTICLE INFO

Article history:
Received 7 October 2008
Received in revised form
2 December 2008
Accepted 19 December 2008
Available online 27 December 2008

Keywords:
PET
Nanofiber
CO_2 laser supersonic drawing

ABSTRACT

Poly(ethylene terephthalate) (PET) nanofibers were prepared by irradiating a PET fiber with radiation from a carbon dioxide (CO_2) laser while drawing it at supersonic velocities. A supersonic jet was generated by blowing air into a vacuum chamber through the fiber injection orifice. The flow velocity from the orifice was estimated by computer simulation; the fastest flow velocity was calculated to be 401 m s^{-1} at a chamber pressure of 6 kPa. A nanofiber obtained using a laser power of 8 W and a chamber pressure of 6 kPa had an average diameter of 193 nm and a draw ratio of about 900,000. This technique is a novel method for producing nanofibers.

1. Introduction

Nanofibers have been produced by electrospinning [1–9], melt electrospinning [10–12], sea-island-type conjugated melt spinning, single-orifice melt blowing, [13] and jet blowing [14]. Out of these methods, electrospinning is the most widely used for preparing nanofibers. Poly(ethylene terephthalate) (PET) nanofibers have been prepared by electrospinning [15] and PET/nylon 6 sea-island conjugated melt spinning [16]. Electrospun PET nanofibers were prepared by spraying a solution of PET–trifluoroacetic acid onto a metallic collector under a high voltage. A PET nanofiber with a diameter of less than 100 nm was formed by PET/nylon 6 sea-island conjugated melt spinning together with laser-heated flow drawing. In this method, the melt-spun fiber was drawn at a draw ratio of 174 by laser heating, and the PET nanofiber was formed by removing the nylon 6 sea component from the drawn conjugated melt-spun fiber.

Recently, we proposed a new approach for producing nanofibers. It involves irradiating a fiber with radiation from a carbon dioxide (CO_2) laser while drawing it at a supersonic velocity. A supersonic jet was generated by blowing air into a vacuum chamber through the orifice used to inject the fiber into the vacuum chamber. The adiabatic expansion of air across the orifice cools the jet. The fiber is instantly melted by the high-power laser beam that irradiates the cold supersonic jet. It is then tremendously deformed by the shear force generated by the supersonic flow, and ultradrawn to a draw ratio of the order of 10^5. We named this preparation method *CO_2-laser supersonic drawing*. Supersonic drawing has already been applied to poly(L-lactic acid) (PLLA) [17] and poly(ethylene-2,6-naphthalate) [18], and in both cases nanofibers were obtained without using any solvent or without removing the second component. The nanofiber obtained by supersonic drawing is basically endless nanofiber because a fiber supplied at a constant speed was continuously laser-irradiated.

The CO_2 laser has been applied to drawing and annealing of various fibers because it can rapidly and uniformly heat fibers. We used the CO_2 laser to draw and anneal fibers and to prepare microfibers. A CO_2 laser-thinning method producing microfibers was previously applied to PET [19], PLLA [20,21], nylon 6 [22], isotactic polypropylene [23] fibers, and their microfibers were obtained, but no fiber of 1 μm or less in diameter was produced by the CO_2 laser-thinning method. Other groups also proposed drawing methods by using the CO_2 laser, but the CO_2 laser drawing methods including our method could not produce nanofibers by using only CO_2 laser-irradiation to fiber [24–26]. On the other hand, the CO_2-laser supersonic drawing can easily prepare various nanofibers by only CO_2 laser-irradiation without combining any process.

In this paper, we prepare PET nanofibers by CO_2-laser supersonic drawing.

* Corresponding author. Tel./fax: +81 55 220 8556.
E-mail address: a-suzuki@yamanashi.ac.jp (A. Suzuki).

0032-3861/$ – see front matter © 2008 Elsevier Ltd. All rights reserved.
doi:10.1016/j.polymer.2008.12.037

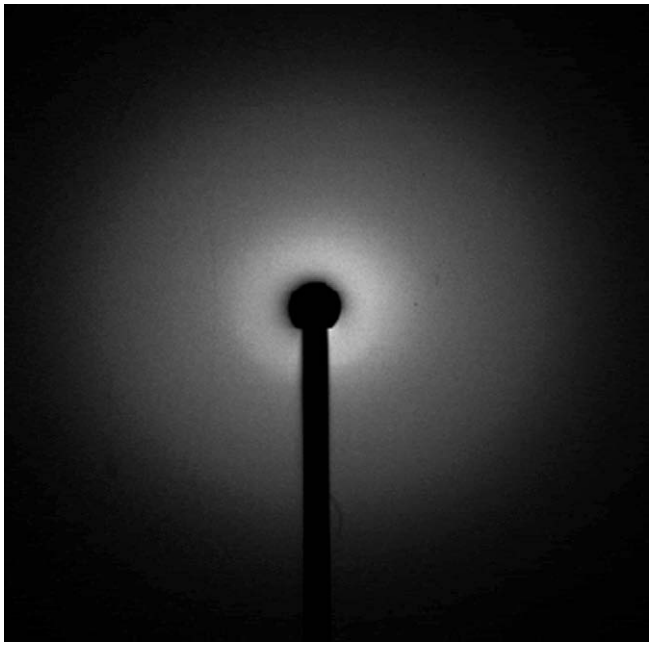

Fig. 1. Wide-angle X-ray diffraction pattern of the original PET fiber.

2. Experimental

The PET fiber used in the present study was prepared from a commercial-grade PET pellet by using a lab melt spinning machine. The as-spun PET fiber had a diameter of 183 μm and a birefringence of 0.27×10^{-3}. It was almost amorphous and isotropic (see Fig. 1). Number- and weight-average molecular weights of this fiber were 3570 and 8380, respectively.

The morphology of the produced nanofiber was determined by scanning electron microscopy (SEM) (JSM-6060LV, JEOL Ltd., Japan) using an accelerating voltage of 10 kV. Before SEM observation, the samples were coated with gold using a sputter coater. The average diameter and the diameter distribution of the nanofiber were measured using an imaging analyzer. The average diameter of a fiber was determined by averaging the diameters measured at 100 locations in a webbed fiber.

The weight-average molecular weight (M_w) and number-average molecular weight (M_n) were measured by gel permeation chromatography (GPC-14, Waters Co.). GPC analysis was performed using two 30 cm gel columns (Shodex HFIP-806M). The measurements were carried out at a column temperature of 40 °C in hexafluoroisopropanol and a flow rate of 0.5 mL/min. A differential refractive-index detector was used as the detector.

Differential scanning calorimetry (DSC) measurements were conducted using a calorimeter (Therm Plus 2 DSC 8230C, Rigaku Co.). The DSC scans were performed within the temperature range 25–280 °C at a heating rate of 10 °C min^{-1}. All DSC experiments were carried out under a nitrogen purge. The DSC instrument was calibrated using indium.

Fig. 2 shows the apparatus used for the CO_2-laser supersonic drawing. It consists of a spool to supply the fiber, a continuous-wave CO_2 laser with an output wavelength of 10.6 μm and a maximum power of 8 W, an acrylic vacuum chamber with Zn–Se windows and a 0.5-mm diameter orifice for injecting the fiber, a power meter, a movable platen, and a vacuum pump. The vacuum chamber was placed on the movable platen that consists of a micro-alignment stage and a laboratory jack that can be moved parallel to the *Y* and *Z* axes allowing the laser irradiation point on the fiber to be finely adjusted.

The velocity distribution from the orifice and the force exerted on the fiber in the air jet were estimated by performing fluid analysis using a three-dimensional (3D) finite element method (FEM) with ANSYS® CFZ 11.0 software.

3. Results and discussion

When performing CO_2-laser supersonic drawing using an air jet, it is very important to determine the velocity distribution in the air

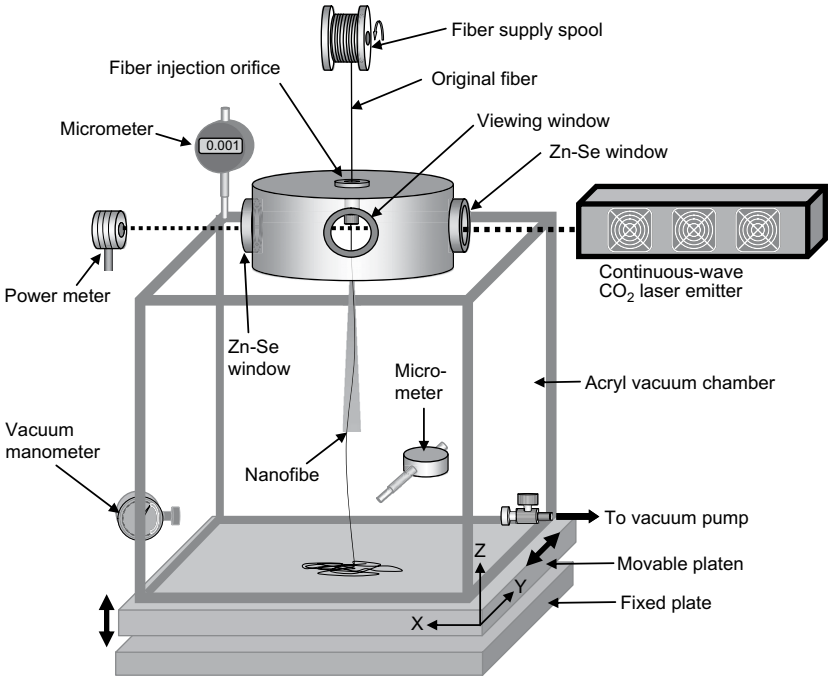

Fig. 2. Schematic diagram of apparatus used for CO_2-laser supersonic drawing.

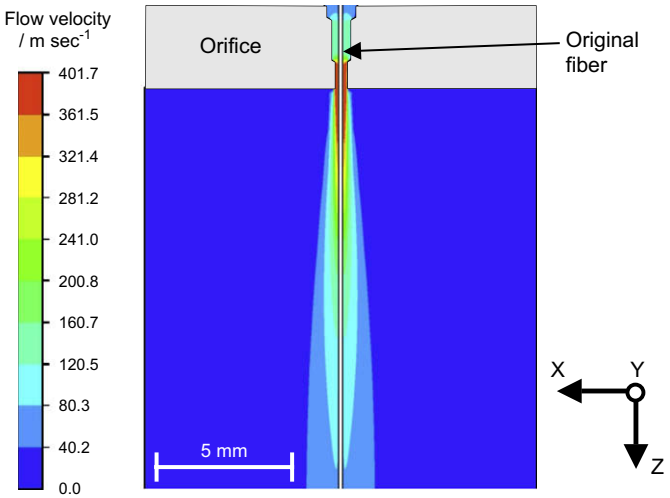

Fig. 3. Flow velocity distribution of the air jet in the *XZ*-plane obtained by the FEM.

jet and the force that is imparted to the fiber surface. A shear force is imparted to the fiber in the supersonic jet in the fluid flow direction and a compressive force is applied in the vertical direction because the airflow is a viscous fluid. The resultant force acts as the drag force to draw the molten fiber to a draw ratio of the order of 10^5 and it determines the fiber diameter and its superstructure. To elucidate the supersonic drawing mechanism it is necessary to analyze the forces applied to the fiber in the air jet.

Fig. 3 shows the flow velocity distribution of the air jet in the XZ-plane calculated by the 3D FEM. This simulation was performed for a chamber pressure of 6 kPa and a 200-μm diameter fiber centered on a 0.5-mm diameter orifice. The flow from the orifice was generated by blowing air into the vacuum chamber to produce a supersonic jet that does not have any accompanying flow that makes the airflow turbulent. This stable airflow generates a fast flow that enables the fiber to be irradiated by the laser beam without causing it to swing. The fastest flow velocities are produced

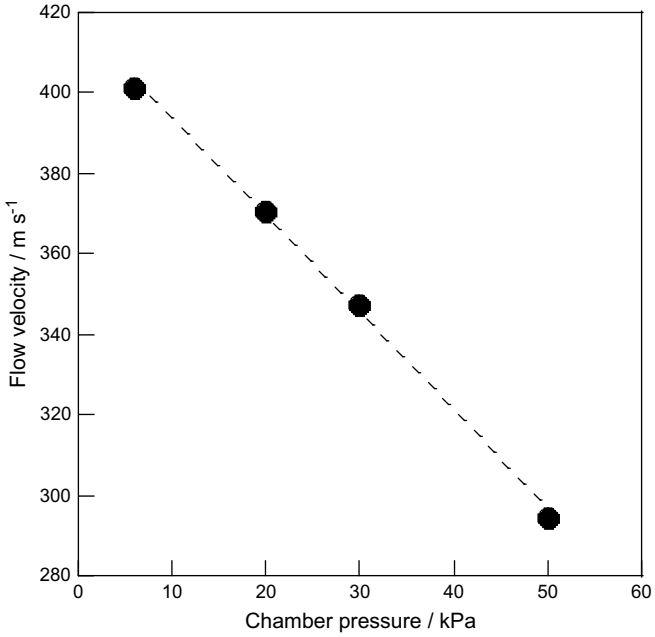

Fig. 4. Flow velocities obtained by the computer simulation at four chamber pressures.

Table 1
Flow velocity (v), Mach number (M), temperature (T) in the supersonic jet at four different chamber pressures (p_{ch}).

p_{ch}/kPa	v/m s^{-1}	M at 298.5 K	T/K
50	295	0.9	261
30	348	1.0	249
20	372	1.1	243
6	402	1.2	235

Sonic speed (C) at 298.5 k: 346.5 ms^{-1}

about 3 mm below the orifice and are in the range 361 and 401 m s^{-1}, making them supersonic. As the distance from the orifice increases, the flow velocity along the fiber decreases rapidly (e.g., the flow velocity at a distance of 14 mm from the orifice is about 40 m s^{-1}). The diameter of the airflow at a distance of 14 mm from the orifice is about 3 mm, and its spread is small.

Fig. 4 shows the flow velocities calculated by computer simulation for four different chamber pressures. The flow velocity increases linearly as the chamber pressure decreases. The maximum flow velocity is 401 m s^{-1} at a chamber pressure of 6 kPa.

The adiabatic expansion of air across the orifice cools the jet. Because the conservation of energy applies along streamlines, the following relation holds between the ratio of the temperature before adiabatic expansion (T_0) to the temperature after adiabatic expansion (T) and the Mach number (M) [27]:

$$\frac{T}{T_0} = \left\{1 + \frac{(\gamma - 1)M^2}{2}\right\}^{-1}, \tag{1}$$

where $\gamma(=C_p/C_v)$ is the ratio of heat capacity at constant pressure (C_p) to that at constant volume (C_v); in the case of air, γ is 1.4 because it consists principally of diatomic gases. The flow velocity is converted into a Mach number by dividing it by the sonic speed at a temperature of T_0:

$$M = \frac{v}{C} = \frac{v}{331.5 + 0.6(T_0 - 273.5)} \tag{2}$$

Table 1 lists the flow velocity (v), Mach number, temperature (T) in the supersonic jet for four different chamber pressures. The flow velocity exceeds the speed of sound only at chamber pressures under 30 kPa. The Mach number at a chamber pressure of 6 kPa is 1.2. The temperature (T) of the supersonic jet at Mach 1.2 is as low as 235 K.

To estimate the drag force acting on the fiber in the supersonic jet, the forces parallel and perpendicular to the surface of the fiber (the shear force and the compressive force, respectively) were analyzed by the 3D FEM. Fig. 5 shows the variation in (a) the shear force and (b) the compressive force which is imparted to the fiber surface in the Z-axis direction as a function of distance from the orifice, and (c) the 3D model used to simulate these forces. The shear force and the compressive force are the values at the nodes along the fiber axis in Fig. 5(c). As the distance from the orifice increases, the shear force decreases rapidly after reaching a maximum value at a distance of 2.2 mm from the orifice. The compressive force is a maximum at the orifice outlet and decreases rapidly with distance from the orifice. The shear force and the compressive force are simultaneously high at about 3 mm from the orifice. The resultant of the shear force and the compressive force is critical for supersonic drawing of a molten fiber heated by a high-power laser beam.

The experimental factors that determine the fiber diameter are the laser power, the chamber pressure, the fiber supply speed, and the laser beam irradiation position. First, the effects of the

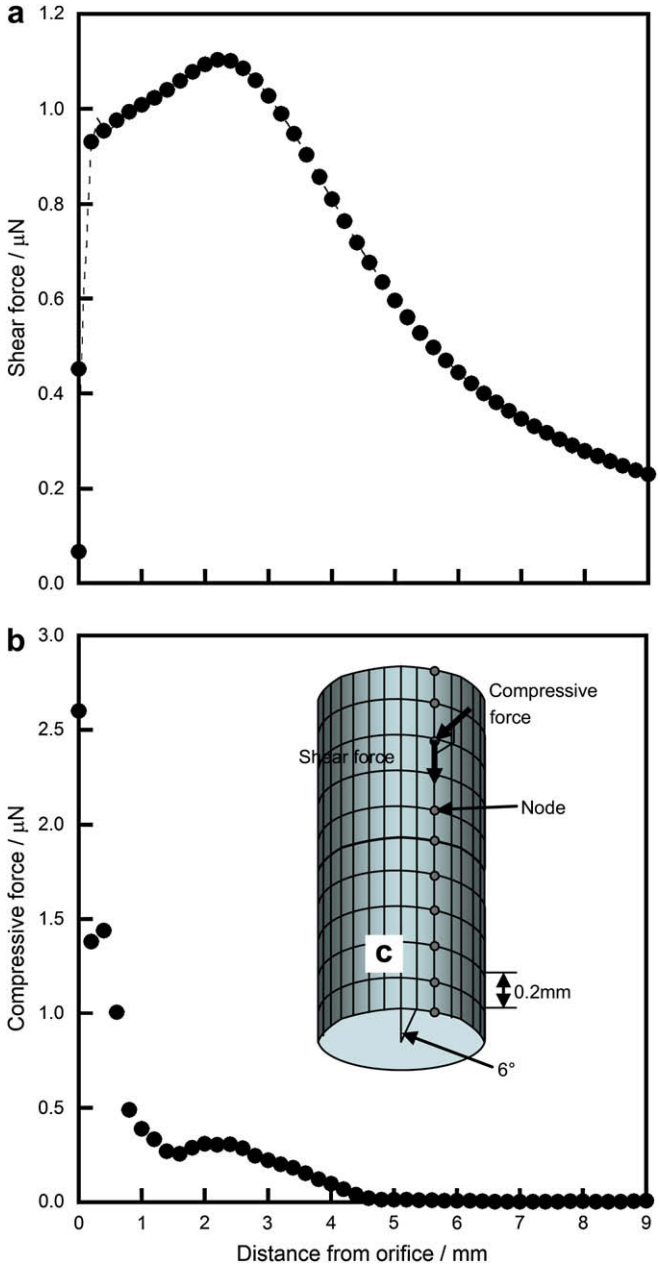

Fig. 5. Variation in the (a) shear force and (b) compressive force at the node of fiber surface in *Z*-axis direction with distance from the orifice, and (c) the 3D model used to simulate the shear force and the compressive force.

laser power, the chamber pressure, and the fiber supply speed on the fiber diameter were investigated. The laser irradiation position was kept constant during a series of experiments; the laser beam was not blocked by the orifice shield at this position. Other details regarding the laser irradiation position are described below.

Fig. 6 shows the dependence of the average fiber diameters at three different laser powers on the chamber pressure. The fiber supply speed was held constant at 0.1 m min^{-1} during this series of experiments. The upper X-axis shows the flow velocity obtained from the linear relation shown in Fig. 4. As the chamber pressure decreases, the average diameter at each laser power decreases significantly; it is less than 1 μm at a chamber pressure of 6 kPa (i.e., at a flow velocity of about 400 m s^{-1}) for all three laser powers. An increase in the flow velocity implies an increase in the drag force. A

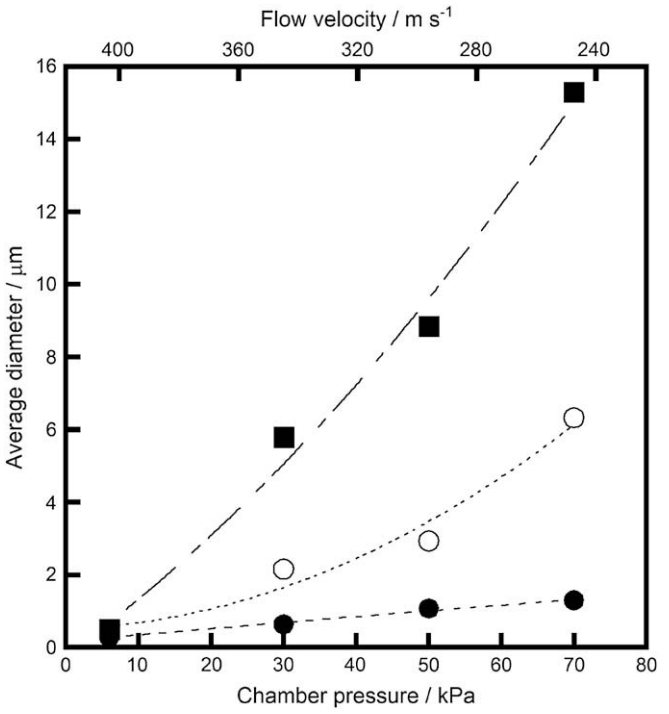

Fig. 6. Chamber pressure dependence of the average diameters obtained at three different laser powers (P_L), ■: $P_L = 4$ W, ○: $P_L = 6$ W, ●: $P_L = 8$ W.

larger drag force induces a higher plastic flow rate, resulting in a thinner nanofiber being produced.

Henceforth, CO_2-laser supersonic drawing was conducted only at a chamber pressure of 6 kPa, at which fibers with diameters below 1 μm can be obtained irrespective of the laser power.

Fig. 7 shows the variation in the average fiber diameter with the supply speed for three different laser powers. As the supply speed is reduced, the fiber diameter at each laser power tends to decrease, and the nanofiber with an average diameter of 313 nm was

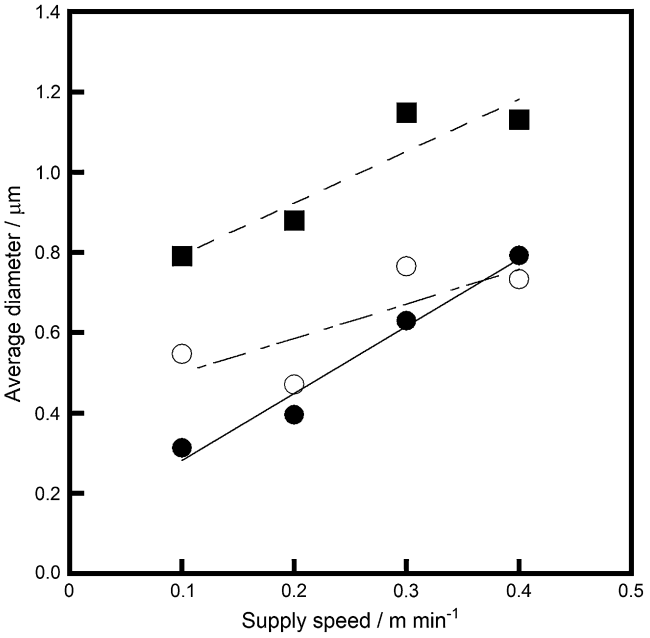

Fig. 7. Variation in the average diameters of the fibers obtained at three different laser powers (P_L) with supply speed, ■: $P_L = 4$ W, ○: $P_L = 6$ W, ●: $P_L = 8$ W.

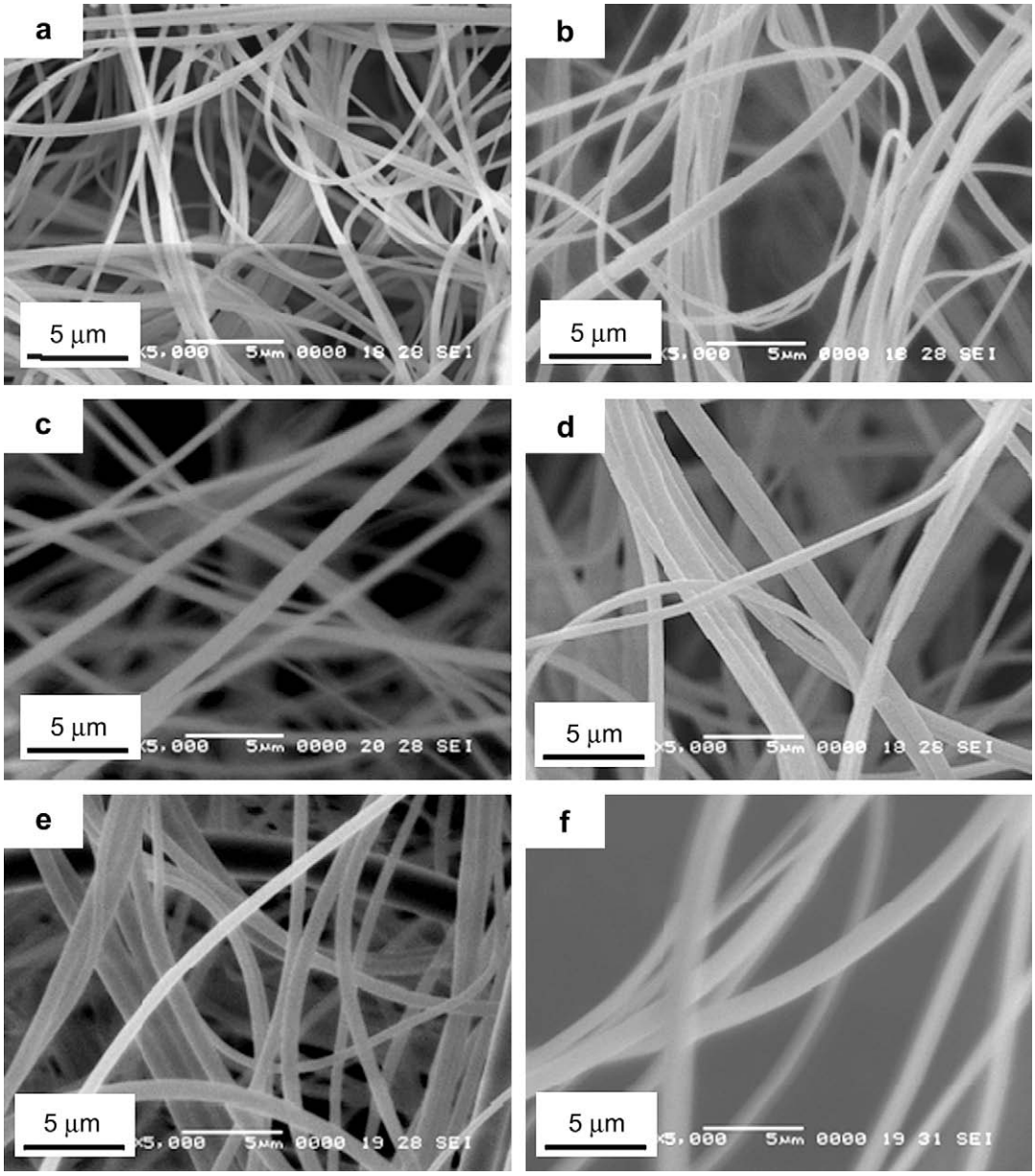

Fig. 8. SEM photographs at magnifications of 5000 for fibers obtained at three different laser powers (P_L) and supply speeds (S_s) of 0.1 and 0.3 m min^{-1}, (a): $P_L = 8$ W, $S_s = 0.1$ m min^{-1}, (b): $P_L = 6$ W, $S_s = 0.1$ m min^{-1}, (c): $P_L = 4$ W, $S_s = 0.1$ m min^{-1}, (d): $P_L = 8$ W, $S_s = 0.3$ m min^{-1}, (e): $P_L = 6$ W, $S_s = 0.3$ m min^{-1}, (f): $P_L = 4$ W, $S_s = 0.3$ m min^{-1}.

obtained when the fiber was supplied at a speed of 0.1 m min^{-1} and was irradiated with a laser power of 8 W. Irradiating at a higher laser power instantly reduces the polymer viscosity, causing the polymer flow rate to increase. Reducing the supply speed, reduces the rate at which polymer mass is supplied to the laser irradiation position. The deformation of the molten polymer increases because the same drag force acts on a smaller mass of polymer that is melted by the laser irradiation.

Fig. 8 shows SEM micrographs at a magnification of 5000 for fibers obtained by varying the laser power and the supply speed. As the laser power is increased and the supply speed is reduced, the reduction in the diameter is confirmed visually by the SEM micrographs. The SEM micrographs reveal that the nanofiber has a smooth surface that has not been roughened by laser ablation and without droplets.

It is well known that the molecular weight is reduced by the thermal degradation that occurs during melt spinning. To investigate whether thermal degradation occurred during irradiation by the CO_2 laser beam, GPC measurements were conducted for a nanofiber produced by CO_2-laser supersonic drawing. Table 2 lists M_w and M_n of the original fiber and the nanofiber obtained by irradiating the laser at a power of 8 W onto a fiber supplied at 0.1 m min^{-1}, and Fig. 9 shows the molecular distributions for these fibers. Laser irradiation causes no noticeable changes in M_w and M_n, and the molecular distribution of the nanofiber is similar to that of the

Table 2
Number-average molecular weight (M_n), weight-average molecular weight (M_w), and M_w/M_n for original fiber and the nanofiber obtained by laser irradiation at a laser power of 8 W and a supply speed of 0.1 m/min.

Fiber	M_n	M_w	M_w/M_n
Original fiber	3570	8380	2.35
Nanofiber	3640	8130	2.23

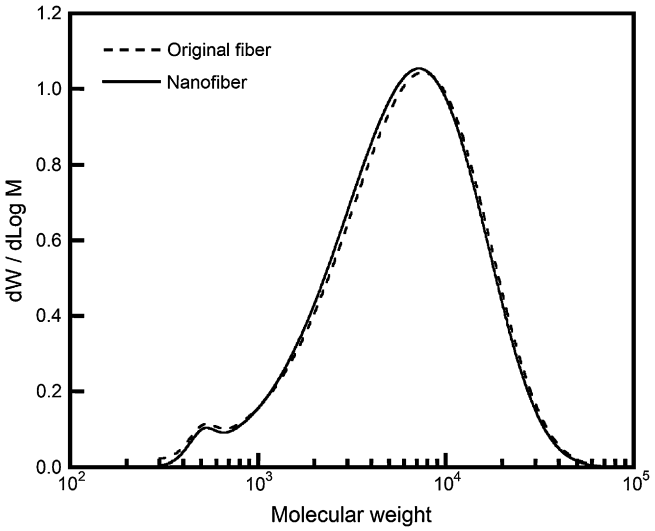

Fig. 9. Molecular distributions of the original fiber and the nanofiber produced at a laser power of 8 W.

original fiber. The GPC results imply that the nanofiber was prepared without thermal degradation induced by irradiation at a high laser power.

Fig. 10 shows the diameter distributions of the fibers obtained at three different laser powers for fiber supply speeds of 0.1 and 0.3 m min^{-1}. As the laser power increases and the supply speed decreases, the diameter distribution gradually becomes narrower, and the average diameter decreases. The thinnest nanofiber produced had an average diameter of 313 nm, a minimum diameter of 177 nm, a maximum diameter of 569 nm, and a standard deviation of 0.078. The thinner the fiber diameter, the higher the uniformity became.

Next, the effect of the laser irradiation position on the fiber diameter was examined. It is very important to investigate this because the shear force and the compressive force depend strongly on the distance from the orifice.

Fig. 11(a) and (b) shows respectively the laser power and the average diameter as a function of the displacement (x) of the vacuum chamber in the Z direction. The laser power, fiber supply speed, and chamber pressure were kept constant at 8 W, 0.1 m min^{-1}, and 6 kPa during the series of the experiments, respectively. When the vacuum chamber was lowered using the laboratory jack in the Z-axis direction and the laser beam operated at 8 W is completely blocked by the orifice shield attached to the vacuum chamber, the displacement is set to $x = 0$. The laser power absorbed by the fiber increases when the vacuum chamber is raised and it becomes constant at a displacement above $x = 3$ mm. This result implies that the actual laser beam diameter is 3 mm, whereas the nominal beam diameter of the CO_2 laser used in this study is 2.4 mm. The nominal beam diameter is defined as the diameter at which more than 90% of the total beam power can be obtained. The laser power near the edge of the beam is weaker than that at the center of the beam because the laser beam has a near-Gaussian profile.

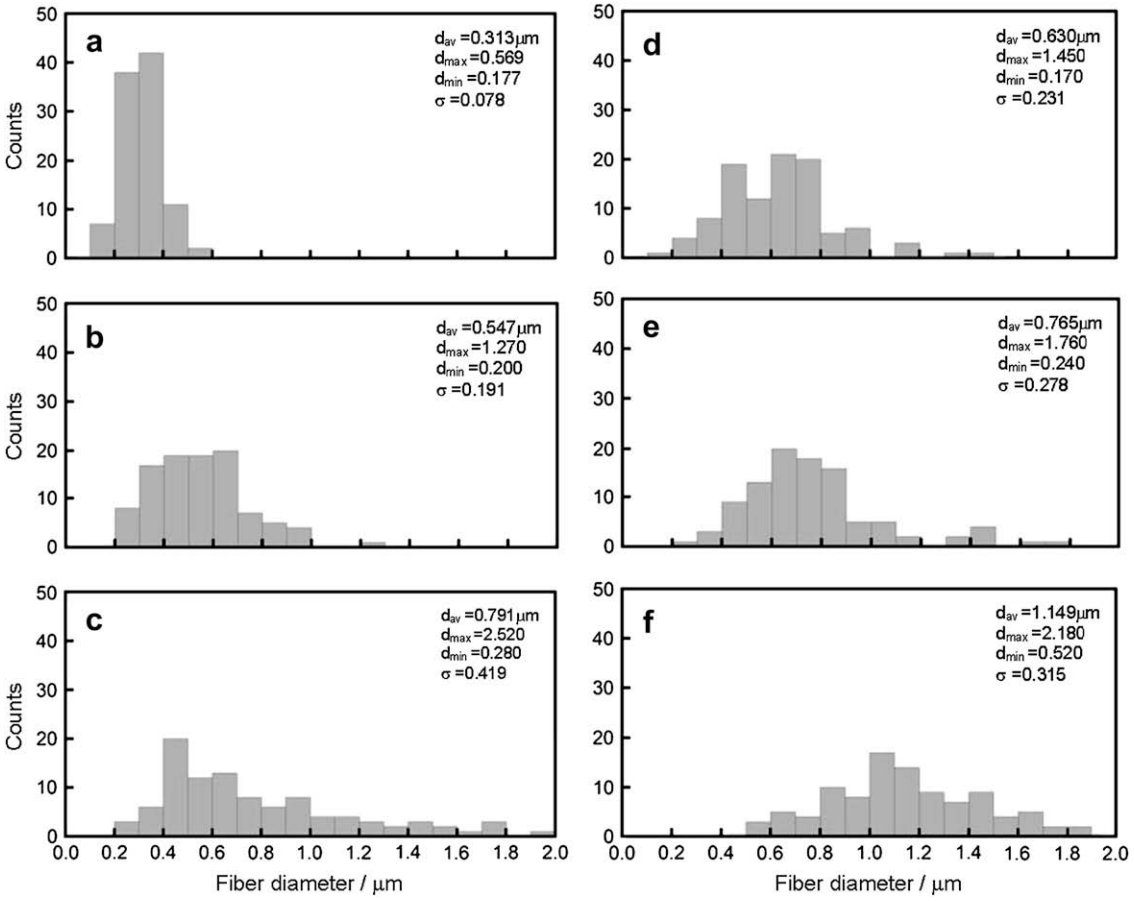

Fig. 10. Diameter distributions of the fibers obtained at three different laser powers (P_L) and supply speed (S_s) of 0.1 and 0.3 m min^{-1}, (a): $P_L = 8$ W, $S_s = 0.1$ m min^{-1}, (b): $P_L = 6$ W, $S_s = 0.1$ m min^{-1}, (c): $P_L = 4$ W, $S_s = 0.1$ m min^{-1}, (d): $P_L = 8$ W, $S_s = 0.3$ m min^{-1}, (e): $P_L = 6$ W, $S_s = 0.3$ m min^{-1}, (f): $P_L = 4$ W, $S_s = 0.3$ m min^{-1}.

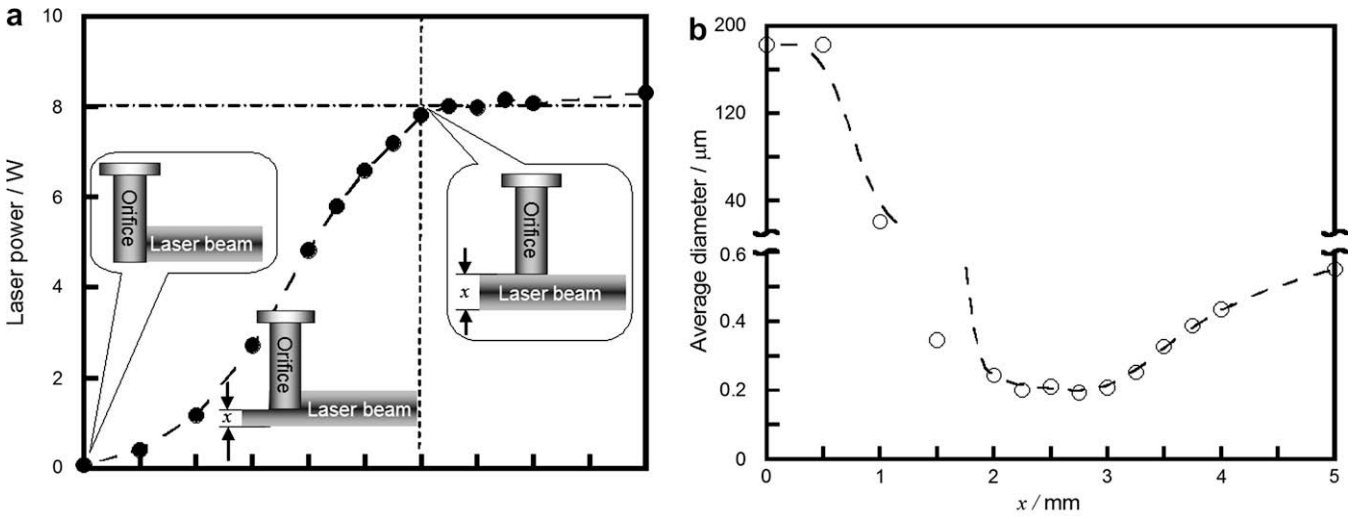

Fig. 11. (a) Relationship between displacement (x) of the orifice in the Z direction and laser power, and (b) the variation in the average diameter with the displacement distance (x).

As the displacement is increased, the fiber diameter initially decreases remarkably and then increases after attaining a minimum diameter of about 200 nm in the x range of 2.0–3.0 mm. The average diameter increases as the laser irradiation position is moved away from the orifice. The thinnest nanofiber was obtained at $x = 2.75$ mm and it had a diameter of 193 nm. The laser power in the range of $x = 0$–1.0 mm is insufficient to produce a thinner fiber since the laser power is lower at the edge of the beam than at the

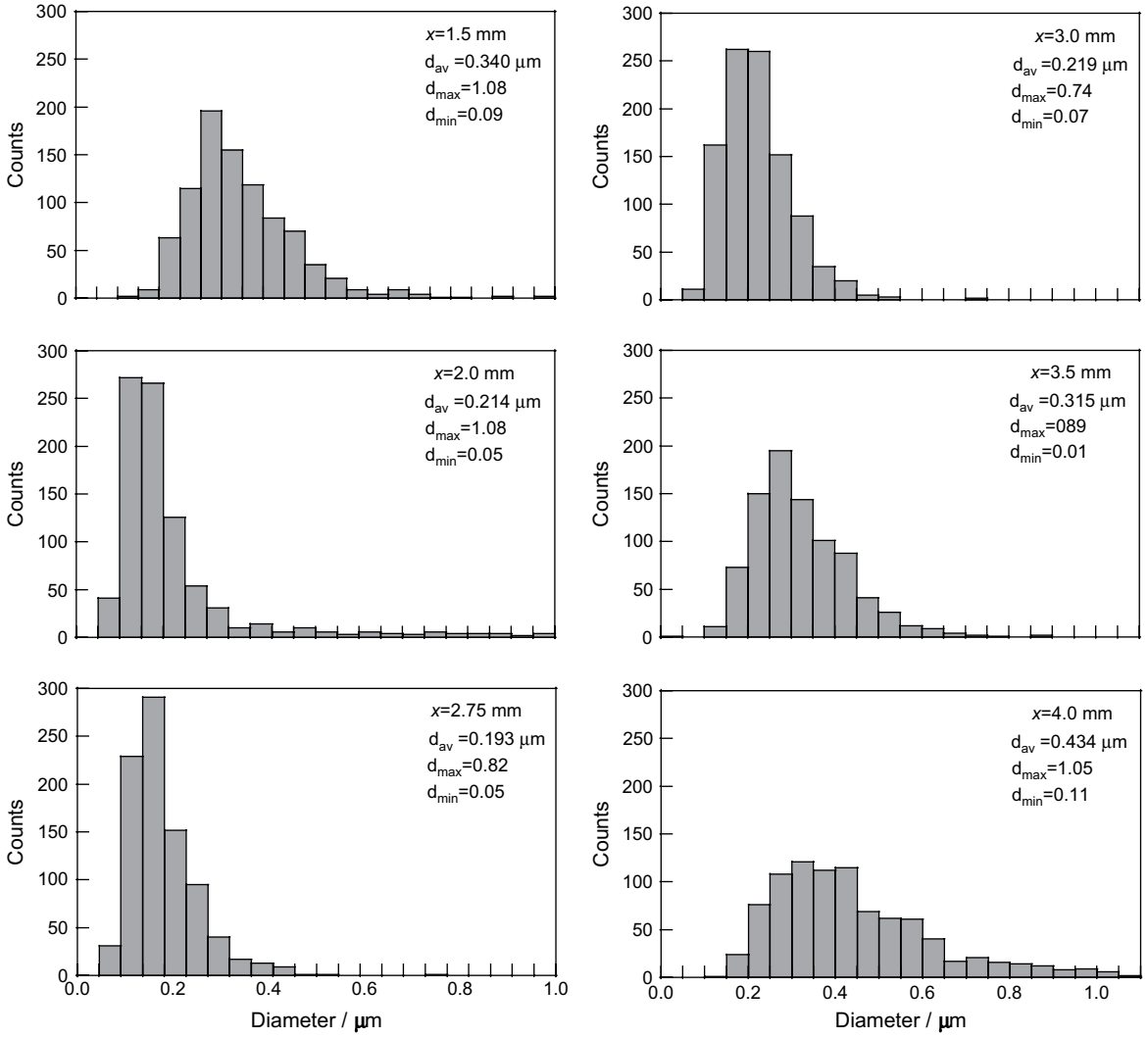

Fig. 12. Diameter distributions of the nanofibers obtained at various displacements (x) of chamber.

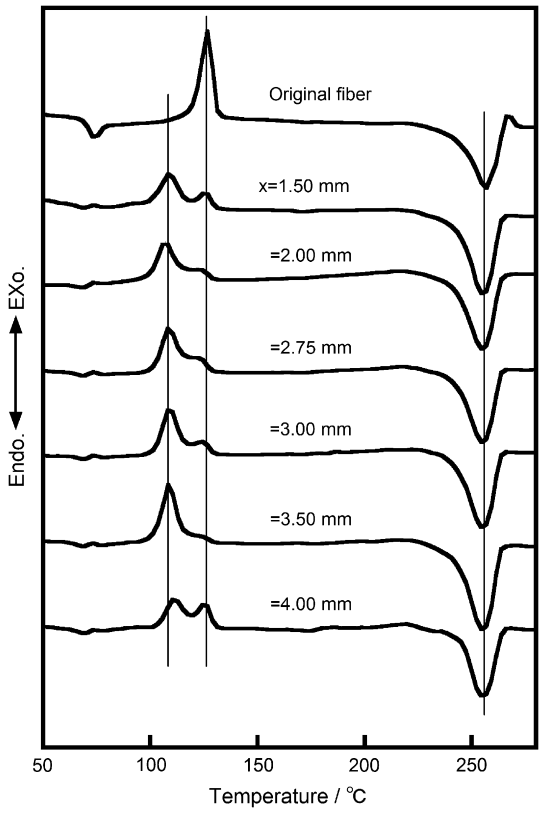

Fig. 13. DSC curves of the original fiber and the original fiber and the nanofibers obtained at various displacements (x) of chamber.

center. The fiber diameter increases as x is increased beyond 3 mm because the shear force decreases rapidly as the distance from the orifice increases (see Fig. 5). In order to obtain a thinner nanofiber it is necessary to irradiate the fiber with a higher laser power at a position where a higher drag force is generated.

The draw ratio (λ) can be calculated easily using the following equation:

$$\lambda = \left(\frac{d_0}{d}\right)^2, \tag{3}$$

where d_0 is the diameter of the original fiber and d is that of the nanofiber, and the volumes before and after drawing are assumed to be equal. The estimated draw ratio of the thinnest nanofiber is about 900,000. A very large plastic deformation occurs momentarily during CO_2-laser supersonic drawing.

Fig. 12 shows the diameter distributions of nanofibers produced at six different displacements and the average (d_{av}), minimum (d_{min}) and maximum (d_{max}) diameters. The thinnest nanofiber obtained at $x = 2.75$ mm has the narrowest diameter distribution. Thin nanofibers with high uniformities can be obtained by laser irradiation for x in the range 2–3 mm. This region is approximately the same as that in which high shear and compressive forces were obtained (see Fig. 5). Even thinner nanofibers should be obtainable by using a higher power laser to irradiate the fiber in the region where a high drag force is generated.

Fig. 13 shows DSC curves of nanofibers obtained at various displacements of the vacuum chamber (x). All the nanofibers and the original fiber exhibit a broad melting endothermic peak at 256 °C. These melting peaks can be ascribed to lamellar crystals, which crystallized during the DSC scanning. Elenga et al. [28] suggested from the standpoint of kinetics that the low-temperature melting peak could be ascribed to the fringed-micelle crystals produced by chain unfolding, and that the high-temperature peak corresponds to the untransformed fraction of the lamellar crystals that undergo reorganization during the heating scan. Fringed-micelle crystals are not present in the nanofibers because the melting peak of the nanofibers was lower than ascribed to lamellar crystals, and it is not visible in the DSC curves.

The original fiber has an exothermic single peak at 127 °C due to cold crystallization. The nanofibers produced at $x = 1.5$ and 4.0 mm have exothermic double peaks at 108 and 127 °C, and the other nanofibers have an exothermic single peak at 108 °C and a shoulder on the high-temperature side of this peak. The shoulder is observed the cold crystallization temperature (T_{cc}) of the original fiber and a higher T_{cc} was obtained for the nanofibers produced at $x = 1.5$ and 4.0 mm. The shifting of T_{cc} to lower temperatures is caused by the increase in the degree of orientation of the amorphous chains and the existence of crystal seeds formed during supersonic drawing. The existence of a double cold crystallization peaks and a single cold crystallization peak with a shoulder suggests that there is difference in the degree of orientation of the amorphous chains. Nanofibers having a broad diameter distribution obtained at $x = 1.5$ and 4.0 mm (see Fig. 12) exhibit double cold crystallization peaks, while nanofibers with a narrow diameter distribution have a single exothermic peak with a shoulder. These results imply that thinner nanofibers have a higher degree of the orientation of the amorphous chains.

4. Conclusion

The PET nanofiber with a uniform diameter was continuously produced by CO_2-laser supersonic drawing. CO_2-laser supersonic drawing could easily produce nanofibers by irradiating a high-power laser beam onto as-spun fibers in a supersonic jet. The resultant force of the shear force and the compressive force generated in the supersonic jet acts as a drag force on the partially molten fiber. A nanofiber with a uniform diameter was obtained when a high-power laser beam is irradiated on the fiber at the position where the drag force is maximized in the supersonic jet. The thinnest nanofiber produced had a diameter of 193 nm and was obtained when the supersonic drawing was carried out at a laser power of 8 W, a chamber pressure of 6 kPa, a fiber supply speed of 0.1 m min^{-1}, and a displacement of 2.75 mm. The laser irradiation at the position where the maximum drag force is obtained causes a large instantaneous deformation, which further thins the fiber resulting in flow-induced orientation and the formation of a nucleus, although flow-induced crystallization does not occur.

CO_2-laser supersonic drawing can be used for all thermoplastic polymers without using any solvent and without removing the second component, and the nanofibers obtained are endless nanofiber because a fiber supplied at a constant speed was continuously laser-irradiated. The CO_2-laser supersonic drawing can easily prepare various nanofibers by only CO_2 laser-irradiation without combining any process. The CO_2-laser supersonic drawing is a new method that nanofiber is produced by using only the CO_2 laser.

Acknowledgment

The authors acknowledge financial support from a Grant-in-Aid for Scientific Research (B) from the Japan Society for the Promotion of Science.

References

[1] Ding B, Kimura E, Sato T, Fujita S, Shiratori S. Polymer 2004;45:1895–902.
[2] Gupta P, Wilkes GL. Polymer 2003;44:6353–9.

[3] Ayutsede J, Gandhi M, Sukigara S, Micklus M, Chen HE, Ko F. Polymer 2005;46:1625–34.
[4] Fong H. Polymer 2004;45:2427–32.
[5] Kim JS, Reneker DH. Polym Eng Sci 1999;38:849–54.
[6] Deitzel JM, Kleinmeyer J, Harris D, Tan BNC. Polymer 2001;42:261–72.
[7] Huang C, Chen S, Reneker DH, Lai C, Hou H. Adv Mater 2006;18:668–71.
[8] Pedicini A, Farris RJ. Polymer 2003;44:6857–62.
[9] Varabhas JS, Chase GG, Reneker DH. Polymer 2008;49:4226–9.
[10] Zhou H, Green TB, Joo Y. Polymer 2006;47:7497–505.
[11] Dalton PD, Grafahrend D, Klinkhammer K, Klee D, Möller M. Polymer 2007;48:6823–33.
[12] Lyons J, Li C, Ko F. Polymer 2004;45:7597–603.
[13] Ellison CJ, Phatak A, Giles DW, Macosko CW, Bates FS. Polymer 2007;48:3306–16.
[14] Borkar S, Gu B, Dirmyer M, Delicado R, Sen AN, Jackson BR, et al. Polymer 2006;47:8337–43.
[15] Hong KH, Kang TJ. J Appl Polym Sci 2006;100:167–77.
[16] Nakata K, Fujii K, Ohkoshi Y, Gotoh Y, Nagura M, Numata M, et al. Macromol Rapid Commun 2007;28:792–5.
[17] Suzuki A, Aoki K. Eur Polym J 2008;44:2499–505.
[18] Suzuki A, Yamada Y. J Appl Polym Sci, in press.
[19] Suzuki A, Okano T. J Appl Polym Sci 2004;92:2989–94.
[20] Suzuki A, Mizuochi D, Hasegawa T. Polymer 2005;46:5550–5.
[21] Suzuki A, Mizuochi D. J Appl Polym Sci 2006;102:472.
[22] Suzuki A, Kamata K. J Appl Polym Sci 2004;92:1454–8.
[23] Suzuki A, Narisue S. J Appl Polym Sci 2006;99:27–31.
[24] Yamaguchi T, Komariyama K, Ohkoshi Y, Urakawa H, Gotoh Y, Terasawa N, et al. J Polym Sci Part B Polym Phys 2005;43:1090–9.
[25] Uddin AJ, Masahima Y, Ohkoshi Y, Gotoh Y, Nagura M, Sakamoto A, et al. J Polym Sci Part B Polym Phys 2006;44:398–408.
[26] Ogata N, Yamaguchi S, Shimada N, Lu G, Iwata T, Nakane K, et al. J Appl Polym Sci 2007;104:1640–5.
[27] Hagena OF. Surf Sci 1981;106:101–16.
[28] Elenga R, Seguela R, Rietsch F. Polymer 1991;32:1975–82.